Experimental performance of an $E \times B$ chopper system

C. Wiesner,[*] M. Droba, O. Meusel, D. Noll, O. Payir, U. Ratzinger, and P. Schneider

Institut für Angewandte Physik (IAP), Goethe-Universität Frankfurt, Max-von-Laue-Str. 1, 60438 Frankfurt am Main, Germany

(Received 4 September 2015; revised manuscript received 25 July 2016; published 22 February 2017)

Beam operation of a novel $E \times B$ chopper system has started in the low-energy beam transport (LEBT) section of the accelerator-driven neutron source FRANZ. The chopper is designed for low-energy high-perveance beams and high repetition rates, and will finally operate with 120 keV protons. It combines a static magnetic deflection field with a pulsed electric compensation field in a Wien filter-type $E \times B$ configuration. The chopper was designed, manufactured and successfully commissioned at the required repetition rate of 257 kHz using a 14 keV helium beam with up to 3.5 mA of beam current. Beam pulses with rise times of (120 ± 10) ns, flat-top lengths of (85 ± 10) ns to (120 ± 10) ns and full width at half maximum (FWHM) between (295 ± 10) ns and (370 ± 10) ns were experimentally achieved.

DOI: 10.1103/PhysRevAccelBeams.20.020101

I. INTRODUCTION

Chopper systems are essential tools to impose a certain time structure on a particle beam. Such time structures are key parameters for the operation of most accelerator facilities. They can be required for low-loss injection or extraction at circular accelerators, to reduce the duty cycle and thus limit the average power deposition for vulnerable machine components, or to create beam-free time intervals for experimental needs such as the time-of-flight (TOF) method.

For the low-energy beam transport (LEBT) section of the accelerator-driven "Frankfurt Neutron Source at the Stern-Gerlach-Zentrum" (FRANZ) [1], a novel $E \times B$ chopper [2] has been designed and successfully commissioned. It combines a static magnetic deflection field with a pulsed electric compensation field in a Wien filter-type $E \times B$ configuration in order to form an ion beam chopper.

In this paper, based on updated results of [3], the chopper requirements, the chopping concept, the optimization of the electric and magnetic fields, as well as numerical and experimental results are presented.

II. CHOPPING REQUIREMENTS FOR FRANZ

The FRANZ facility is currently under construction at Frankfurt University. It will deliver neutrons in the energy range of 1 keV to 500 keV, which are especially suited for nuclear astrophysics experiments [4]. The neutron production using the $^7\mathrm{Li}(p,n)^7\mathrm{Be}$ reaction requires a 2 MeV primary proton beam. An overview of the facility is given in Fig. 1.

The main operation mode of the facility is the time-of-flight or compressor mode. It requires a pulsed beam for the energy-dependent measurements of neutron capture cross sections. In this case, beam pulses with at least a 50 ns flat-top at a repetition rate of 257 kHz have to be shaped in the LEBT section at a beam energy of $W_\mathrm{b} = 120$ keV.

The LEBT section is based on four solenoids with the chopper located between Solenoid 2 and Solenoid 3. The chopped beam is then accelerated by a compact linac operating at a frequency of $f_\mathrm{rf} = 175$ MHz. The linac consists of a 4-rod type Radio-Frequency Quadrupole (RFQ), providing acceleration to 700 keV, and an IH drift-tube cavity that provides acceleration to the design energy of 2 MeV [5]. In front of the neutron production target, a bunch compressor [6] generates 1 ns short pulses for the TOF measurements.

III. CHOPPER CONCEPTS

The FRANZ ion source is designed to provide a dc proton beam current of $I_\mathrm{b} = 50$ mA, with possible upgrades to 200 mA [7]. Pulsing the ion source to generate the time structure is not considered a feasible option. On the one hand, the plasma build-up time for a stable proton beam is higher than the required pulse repetition time of $(257\ \mathrm{kHz})^{-1} \approx 4\ \mu$s. On the other hand, it is not feasible to pulse the extraction system due to the significant power deposition on the extraction electrode when operated with high repetition rates and high beam currents.

Consequently, a dedicated chopper system is required. In order to reduce the beam loading for the accelerating structures, the chopper is placed in the low-energy part, before the beam is injected into the RFQ. Therefore, the first question is whether any of the existing chopper

[*] wiesner@iap.uni-frankfurt.de

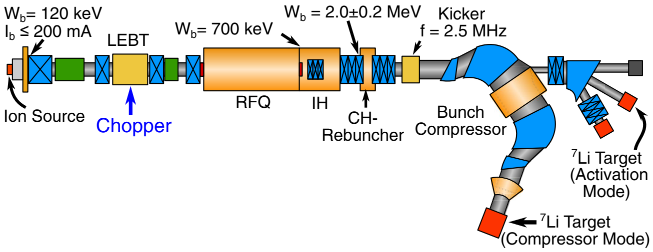

FIG. 1. Schematic overview of the Frankfurt neutron source FRANZ. The chopper is located in the center of the LEBT section.

concepts for low-energy beam transport sections are feasible for the FRANZ operation parameters.

Mechanical choppers, like disk choppers [8,9] or Fermi choppers [10,11], which are widely used for noncharged particles, have typical operation frequencies in the sub-kilohertz range, which are too low for the FRANZ case. An alternative concept is to charge the central electrode of an Einzel lens to higher voltage than the accelerating voltage of the beam, thus reflecting the beam [12,13]. However, for the relatively high initial beam energy of 120 keV and the high repetition rate required for FRANZ, this concept does not seem feasible.

A different approach would be to change the properties of the undesired beam such that it ceases to fit into the acceptance of subsequent accelerator structures and gets lost. This can be implemented by modulating the beam energy so that the undesired beam no longer fits into the longitudinal acceptance of the RFQ [14] or by superposing a transverse momentum so that the beam is mismatched to the transverse acceptance of the RFQ [15]. In these cases, no beam dump and only relatively low fields are required. However, since the undesired beam is lost in the RFQ, this is only practical for small average beam power. For the FRANZ LEBT, with a dc beam power of $P_b = \frac{W_b}{e} \cdot I_b = 120\ \mathrm{kV} \cdot 50\ \mathrm{mA} = 6\ \mathrm{kW}$, the additional losses on the RFQ electrodes would not be acceptable.

A standard chopper solution in many facilities [16–19] is the use of transverse electric kickers to deflect the beam from the reference trajectory. This requires that an electrostatic field is built up during the beam-interception time or that an oscillating field is produced by an rf cavity or a resonant circuit. For a repetition rate of 257 kHz, an rf cavity as well as a resonant circuit is technically challenging due to the large dimensions that would be needed. In addition, this solution can lead to emittance growth from the transverse beam oscillation [20], which would have to be reduced using a more complex setup, e.g., superposing a higher harmonic frequency [21].

Nonresonant electric kickers, however, require insulated deflection electrodes or plates. This bears the risk of sputtering [22] as well as sparking and high-voltage (HV) breakdowns [23–25], which can become an issue for high-intensity beams [26,27]. In contrast, a magnetic kicker would deflect the beam reliably, without risk of voltage breakdowns, but would consume too much power and would be challenging to operate at 257 kHz.

Therefore, the idea for the FRANZ chopper is to combine an electric kicker with a perpendicular, static magnetic field to form a single device called $E \times B$ chopper [2,3]. A scheme of the chopper system and its main components is shown in Fig. 2. The incoming dc beam is continuously deflected by the static chopper magnet. Then a pulsed electric field is used to compensate the magnetic deflection and to create a beam pulse in the forward direction. It is, to our knowledge, the first time that this concept is used to chop ion beams. However, a similar concept was previously employed to reduce the duty cycle of a low-energy electron beam for the Low-Energy Undulator Test Line (LEUTL) in the Advanced Photon Source (APS) at Argonne National Laboratory [28].

In the present setup, discussed in this paper, the beam will be dumped directly on the vacuum chamber that is located downstream of the chopper. For a future high-power upgrade, a dedicated beam-separation system will be

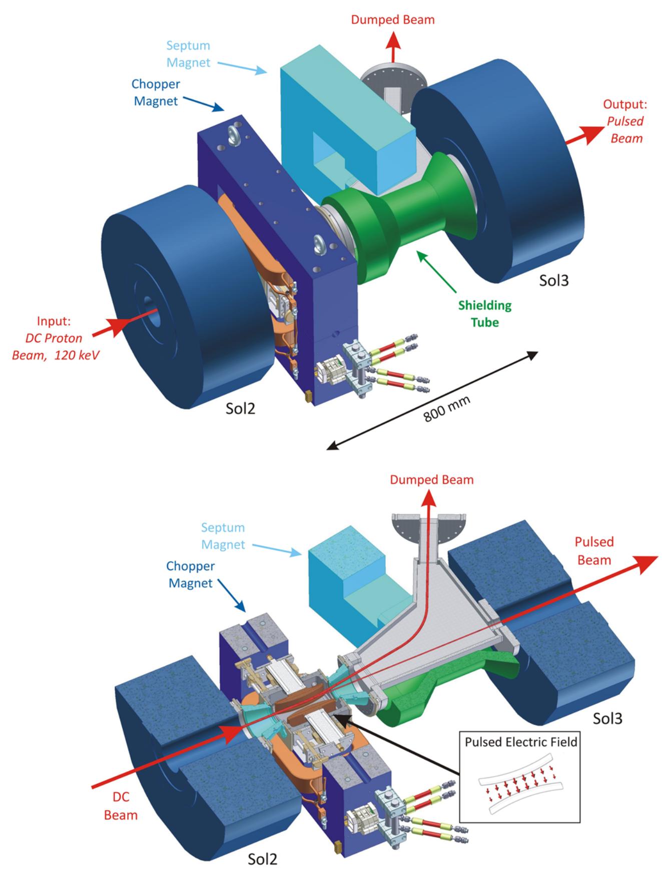

FIG. 2. Schematic overview of the $E \times B$ chopper: perspective view (top) and cross sectional view (bottom). The chopper is installed in the LEBT section between Solenoid 2 and 3. Figure was modified from [29]. The total length, including the beam-separation system, is 80 cm.

installed behind the chopper dipole, as shown in Fig. 2. The beam-separation system will use a massless septum magnet to minimize the power deposition on the vacuum chamber as well as the uncontrolled production of secondary particles.

The $E \times B$ concept combines the advantages of magnetic deflection, i.e., stable deflection without risks of voltage breakdown, and of electric deflection, i.e., operation with low power consumption even at high repetition rates. In this setup, however, the beam pulse is exposed to the full electric and magnetic fields. Therefore, a careful global and local matching of the electric and the magnetic deflection forces is required to avoid beam offsets and to ensure a high beam quality.

IV. FIELD OPTIMIZATION

A particle with charge q and velocity v_z will not exit an $E \times B$ system (with magnetic field B_y and electric field E_x) with any additional transverse momentum if the Wien condition [30]

$$\int q \cdot (E_x - v_z \cdot B_y) dz \stackrel{!}{=} 0 \tag{1}$$

is satisfied in the integral form. However, this is not sufficient to assure an unperturbed beam trajectory throughout the system. In addition, the magnetic and electric deflection forces must be also *locally* matched.

Initially, the deflection forces must be longitudinally matched on the beam axis in order to avoid horizontal deviations from the beam axis and a position offset behind the $E \times B$ system. This is achieved by installing shielding tubes that shorten the magnetic field and by longitudinally optimizing the pole contour of the dipole [3,31]. The resulting dipole cross section is depicted in Fig. 3.

In a next step, the deflection forces have to be matched in the transverse planes by optimizing the $x - y$ pole contour. Two changes in the pole contour are required.

First, the longitudinal velocity $v_z(x)$ of the off-axis particles changes in the electric potential of the symmetrically charged deflection plates. This leads to a focusing effect in the horizontal plane [3,33]. The velocity change can be compensated by modifying the B field so that the magnetic force

$$\vec{F}_{\text{mag}} = q \cdot v_z(x) \cdot B_y(x) \tag{2}$$

remains constant for all x positions. A partial compensation can be used to distribute the focusing effect equally in both transverse planes, thus preserving a given cylindrical symmetry of the beam [3,33,34].

Second, the magnetic field distribution has to be adapted to possible inhomogeneities in the electric field distribution. Therefore, a parabolic term is added. In superposition,

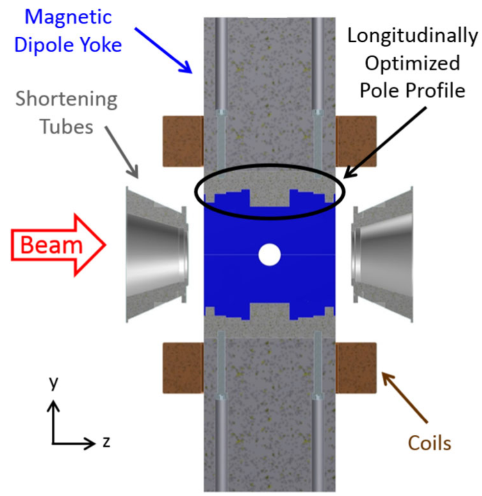

FIG. 3. Cross section of the chopper dipole in the $y - z$ plane. Shortening tubes and a longitudinally optimized pole profile are used to match the shapes of magnetic and electric deflection forces [3,32].

the analytic expression for the dipole contour with gap height h_{gap} is given by

$$y(x) = \frac{1}{2} h_{\text{gap}} \cdot \frac{1}{\sqrt{1 - b \cdot \frac{E_x}{V_{\text{acc}}} \cdot x}} - c \cdot x^2, \tag{3}$$

with the longitudinal acceleration voltage V_{acc} and the electric deflection field E_x. The parameters b and c can be fitted for nonideal cases like high dipole gaps [3,33]. For the field simulations the commercially available code CST EM Studio was used [35]. More details on the optimization process can be found in [3].

Figure 4 shows a picture of the chopper dipole with the transversely and longitudinally optimized pole contour. A beam that is transported through these fields preserves its cylindrical symmetry and does not experience additional emittance growth.

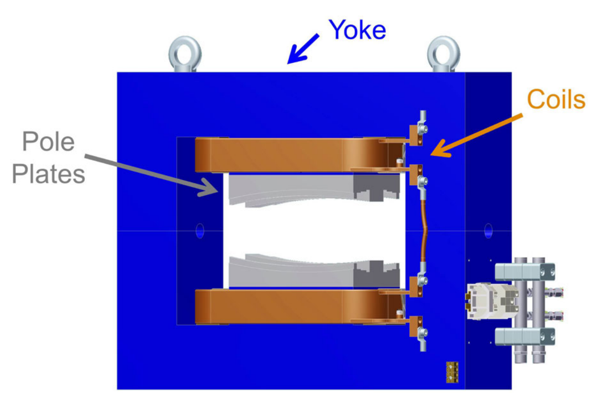

FIG. 4. Chopper dipole with transversely and longitudinally optimized pole contour. The beam direction is perpendicular to the dipole front plane shown.

V. BEAM DYNAMICS SIMULATIONS

Based on the optimized field configuration, beam dynamics simulations for the 120 keV proton beam were performed using the Particle-in-Cell (PIC) code BENDER [36].

The optimized field setup of Sec. IV was used and the measured HV pulse shape was imported into the simulations. Different time steps of the beam shaping simulation are given in Fig. 5. The projection on the $z-x$ plane is shown. The 120 keV dc beam enters the chopper from the left side. It is composed of 50 mA protons (depicted in blue), as well as the undesired hydrogen fractions: 5 mA H_2^+ ions (red) and 5 mA H_3^+ ions (dark green). These values for the undesired fractions are a worst-case assumption. They will later be reduced by installing a collimator system in front of the chopper. Transport simulations show a reduction by more than 60 % for H_2^+ and more than 70 % for H_3^+ ions before the chopper for the standard solenoid settings.

At $t = 20$ ns the beam is statically deflected by the magnetic field and dumped at the vacuum chamber. In the magnetic field, the three hydrogen fractions are separated by their momentum. The beam-separation system was not included in the simulation. Part of the H_2^+ and H_3^+ ions but no protons are lost on the deflection plates.

At $t = 480$ ns the electric field compensates the magnetic deflection for the proton beam, so that the protons can traverse the circular aperture. The slower H_2^+ and H_3^+ ions are bent in the direction of the electric field. During the fall time of the electric field ($t = 620$ ns and $t = 780$ ns), the dc beam returns to its initial position, while the pulse propagates through the second part of the LEBT. Solenoids 3 and 4 are used to match the proton pulse into the acceptance of the RFQ. Note that the latter was not included in this simulation. Most of the remaining H_2^+ and H_3^+ ions have very high position offsets and can later be removed by a collimator system in front of the RFQ.

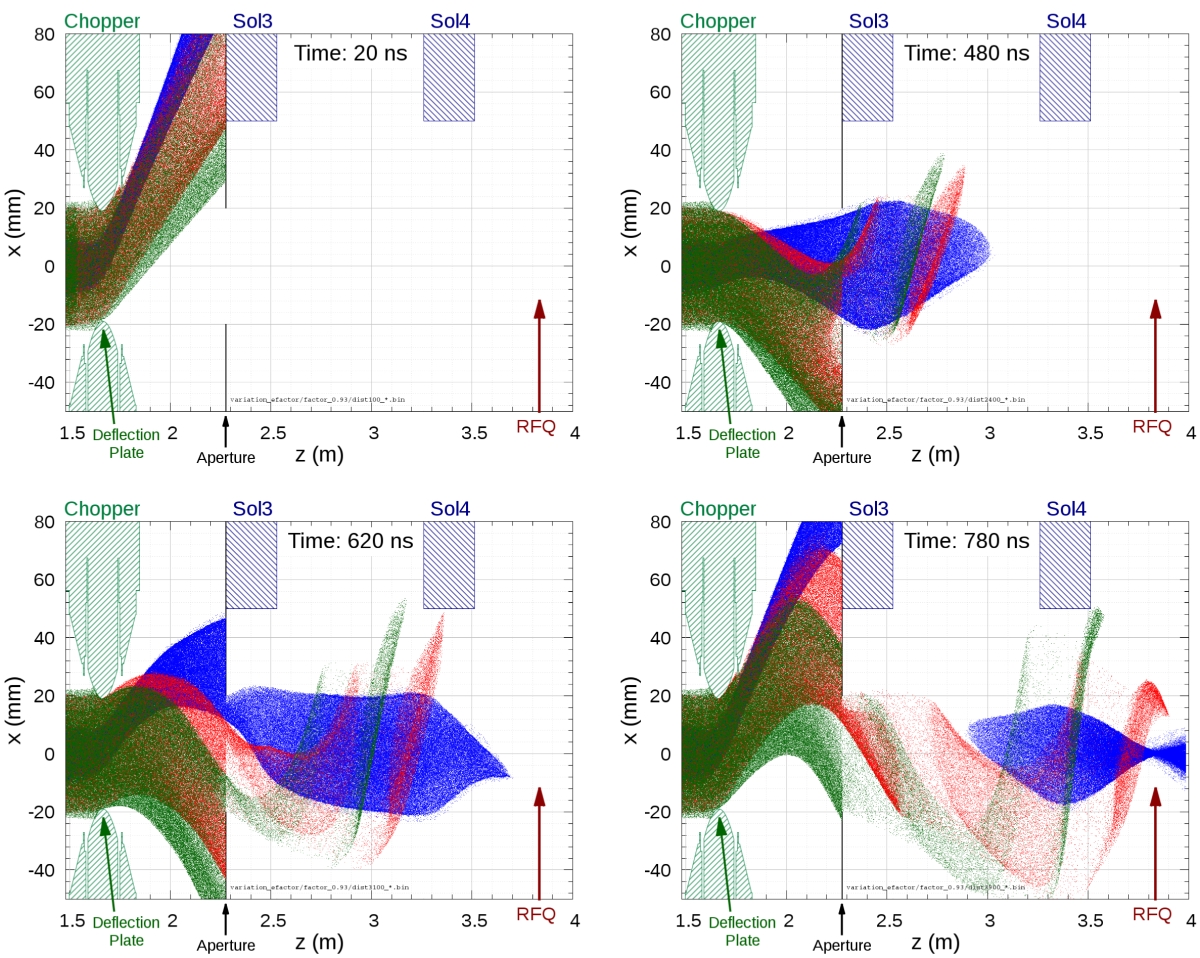

FIG. 5. Different time steps of a beam shaping simulation in the $E \times B$ chopper [3]. The dc beam enters the chopper from the left side. It is composed of 50 mA protons (depicted in blue), 5 mA H_2^+ ions (red) and 5 mA H_3^+ ions (dark green). The beam energy is 120 keV. The measured HV pulse is imported into the simulation and used to ramp the electric field. The proton pulse is shaped at a circular aperture with a 20 mm radius. The solenoids used for transverse focusing are shown in blue. The electric deflection plates and the repeller electrodes are depicted in green.

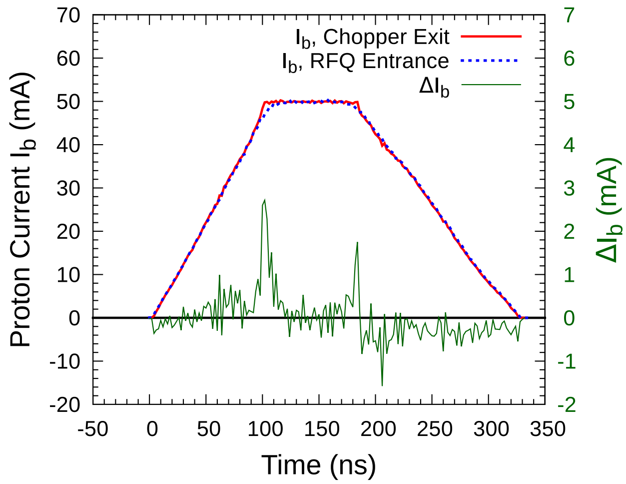

FIG. 6. Simulated pulse shape for 120 keV protons directly behind the chopper (red) and at the RFQ entrance (blue). The difference $\Delta I_b = I_b^{\mathrm{chopper}} - I_b^{\mathrm{rfq}}$ is depicted in green. No relevant increase of the pulse length is observed.

The resulting proton pulse shape is depicted in Fig. 6. The time requirements of at least a 50 ns flat-top length and a maximum total length of 350 ns are fulfilled. No significant increase of the pulse length is observed during the transport from the chopper to the RFQ, located 1.5 m downstream. Note that the fall time is slightly larger than the rise time due to the asymmetric shape of the primary HV pulse.

The particle distribution behind the chopper shows that the emittance growth is reduced to the same level as in a simple drift. In addition, the matched chopper fields do not produce any beam offset, nor a significant ion redistribution. Moreover, the beam pulse can benefit from the moderate focusing properties of the Wien filter [3].

VI. MANUFACTURE OF THE CHOPPER SYSTEM

The optimized chopper components were manufactured at IAP and by external companies. A picture of the chopper magnet, including the main dimensions, is shown in Fig. 7.

TABLE I. Main parameters of the chopper magnet.

Parameter	Value
Yoke length	150 mm
Length incl. coils	244 mm
Gap height	110 mm
Number of turns N per coil	48
Coil current I_{dipole}	130 A
Excitation field $N \cdot I_{\mathrm{dipole}}$	12480 A-turns
Max. field on axis B_0	146 mT
Current density j	5.6 $\mathrm{A\,mm^{-2}}$

An H-type dipole with a 150 mm length is used. Exchangeable pole plates allow the electric and magnetic deflection forces to be matched also for future changes of the deflection plate geometry. A relatively high gap of 110 mm is required to accommodate the electric deflection unit. The main parameters of the chopper magnet are listed in Table I. In the standard operation mode, a field of $B_0 \approx 60$ mT is used for a 10° beam deflection.

The electric field is generated between two deflection plates made of copper. The longitudinal shape of the plates is adapted to the beam envelope. Shims at the top and the bottom improve the transverse field homogeneity. The water-cooled plates are mounted on cylindrical insulators. The horizontal distance between the center of the plates can be varied between $d_0 = 20$ mm and $d_0 = 80$ mm using a customized translator system. A scheme of the electric deflection unit is shown in Fig. 8.

The field is driven by a HV pulse generator, which was developed at IAP. It uses fast MOSFET technology in the primary circuit, while the high voltage is provided in the secondary circuit by a ferrite transformer core. Electrode voltages of up to ±4.9kV are reached *in situ* with 257 kHz repetition rate. The main parameters of the electric deflector are summarized in Table II.

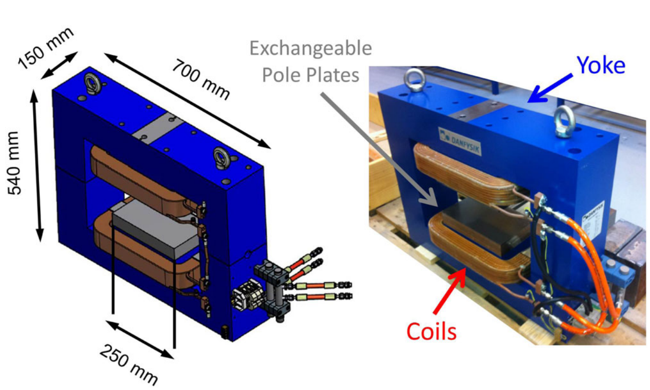

FIG. 7. Drawing (left) and photograph (right) of the chopper dipole.

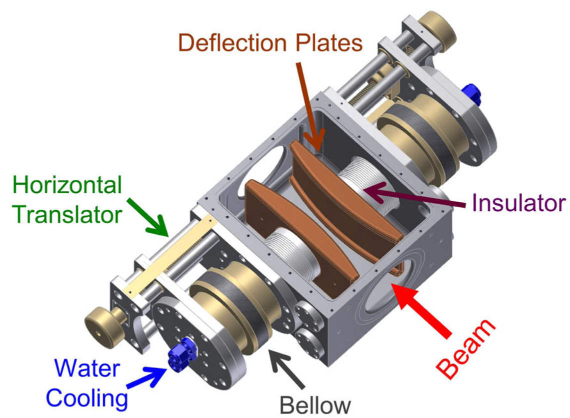

FIG. 8. Main components of the electric deflection unit for the $E \times B$ chopper.

TABLE II. Main parameters of the electric deflection unit.

Parameter	Value
Length of deflection plates	150 mm
Height of deflection plates	80 mm
Pulsed voltage amplitude V_0	±4.9 kV
Pulse repetition rate	257 kHz

VII. BEAM EXPERIMENTS

A. Experimental setup

An overview of the FRANZ LEBT section, as used for the beam experiments presented in this section, is given in Fig. 9.

Four solenoids are used for transverse focusing. The chopper is installed between Solenoids 2 and 3 in the center of the LEBT section. The HV pulse generator is installed above the chopper.

The beam pulse is shaped at a circular aperture with a radius of 50 mm. For the future 120 keV proton beam, a smaller aperture with a 20 mm radius will be employed. For commissioning, a filament-driven volume type ion source was operated with a He^+ beam at 14 keV energy. The beam pulse is measured at a fast beam current transformer (BCT) installed between the third and fourth solenoid. In front of and behind the chopper, negatively biased electrodes repel electrons from the deflection area. A photograph of the low-energy line and the $E \times B$ chopper after assembly is shown in Fig. 10.

B. Repetition rate and pulse shape

Beam repetition rates between 103 kHz and 257 kHz can be experimentally achieved for the given setup by adapting the trigger pulse of the HV pulse generator. The measured beam pulses are shown in Fig. 11.

Beam pulses with rise times of (120 ± 10) ns, flat-top lengths of (85 ± 10) ns to (120 ± 10) ns and full width at half maximum (FWHM) between (295 ± 10) ns and (370 ± 10) ns were achieved [3]. In this case, the flat-top length is defined as the time difference between the 98 %

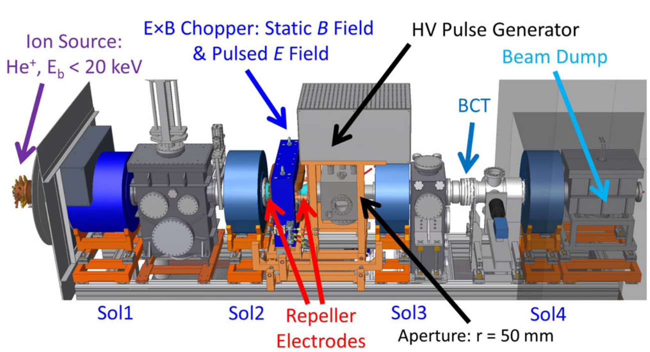

FIG. 9. Overview of the FRANZ LEBT section, as used for the experiments presented in this section.

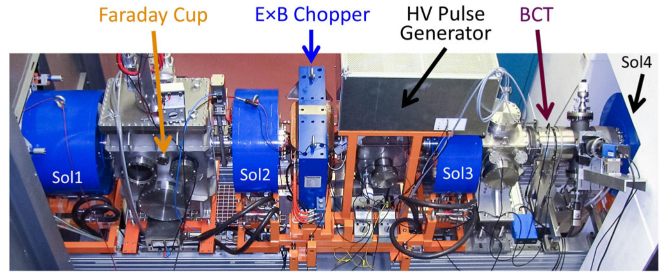

FIG. 10. FRANZ LEBT section, including the $E \times B$ chopper.

amplitude values. For a given aperture, the beam pulse length could be modified by varying the beam size at the aperture position.

An almost identical value for both the peak transmission of the chopped beam and the transmission of the dc beam could be achieved by adjusting the solenoid field strength: the pulse amplitude, measured at the BCT, corresponds to (95.2 ± 1.6) % of the maximum transmitted dc current value, measured at the Faraday Cup behind Solenoid 4.

Due to the repeller electrode in front of the chopper system, the space-charge compensation [37–40] can be preserved in the first part of the LEBT, i.e., between the ion source and the chopper entrance. In contrast, in the second

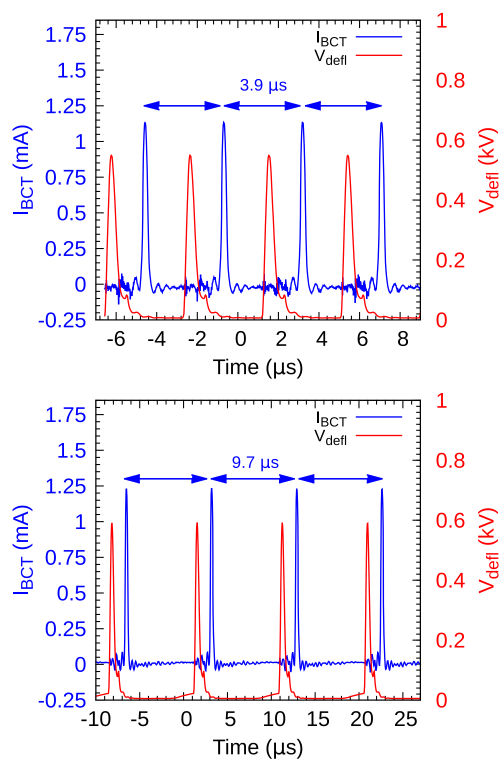

FIG. 11. Measured 14 keV He^+ beam pulses with a repetition rate of 257 kHz (top) and 103 kHz (bottom). The signal of the BCT I_{BCT} is depicted in blue and the voltage V_{defl} at the positively charged deflection plate in red. The original BCT data without rf noise correction or baseline restoration are shown.

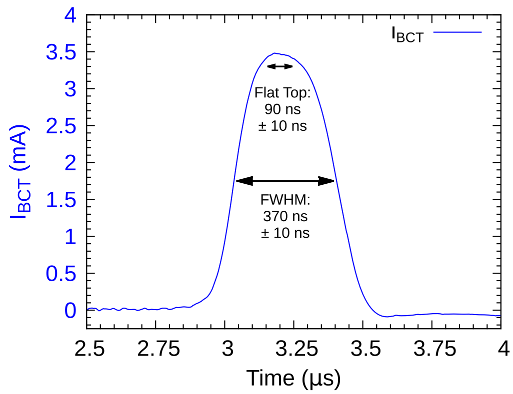

FIG. 12. Measured 14 keV He^+ beam pulse with 3.5 mA amplitude. The baseline of the BCT signal was manually restored.

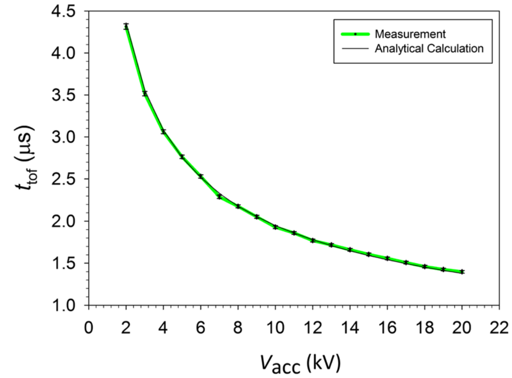

FIG. 13. Measured (green) and analytically calculated (black) time of flight t_{tof} between the center of the deflection plates and the BCT for the He^+ pulses as a function of the accelerating voltage V_{acc}.

part of the LEBT, i.e., between the chopper exit and the RFQ entrance, no space-charge compensation can be expected for the pulsed beam. The reason is that the build-up time for the space-charge compensation (due to residual gas ionization) is much longer than the flight time of the beam pulse from the chopper to the RFQ [3] [Chap. 5.3]. Therefore, the beam pulse has to be transported with full space charge in this part of the LEBT section.

He^+ beams with beam currents of up to 3.5 mA, limited by the given test ion source, were successfully chopped and transported. This corresponds to a generalized perveance of 2.7×10^{-3}. For the design species and energy, 120 keV protons, this is equivalent to a beam current of 175 mA. A measured beam pulse with 3.5 mA amplitude is shown in Fig. 12.

During the measurements, the BCT was exposed to the rf noise that was emitted by the HV pulse generator. This effect is still visible in Fig. 11. In the future, a better shielding of the pulse generator and the BCT cables will be used to further reduce the noise level.

C. Time of flight

The chopped beam pulse reaches the BCT after a certain time of flight:

$$t_{\mathrm{tof}} = \frac{d_{\mathrm{tof}}}{v_0}. \tag{4}$$

For the given setup, the distance between the center of the BCT and the center of the deflection plates is $d_{\mathrm{tof}} = (1349 \pm 2)$ mm.

The nonrelativistic velocity v_0 of a particle with mass m_{p} can be determined directly from the accelerating voltage using:

$$v_0 = \sqrt{2 \cdot V_{\mathrm{acc}} \frac{q}{m_{\mathrm{p}}}}. \tag{5}$$

This way, the analytically calculated time of flight can be compared to the measured time of flight. The latter is given by the time difference between the center of the primary HV pulse and the center of the beam pulse. The measured and the analytically calculated values are shown in Fig. 13 for different beam energies $W_{\mathrm{b}} = e \cdot V_{\mathrm{acc}}$ between 2 keV and 20 keV [3]. Here, the center of the beam pulse was defined as the center of the 90 %-amplitude values from the BCT measurement.

In these measurements, the indicated error for t_{tof} results from the 5 ns time resolution of the oscilloscope, from possible uncertainties in the extraction voltage and in the exact distance as well as from the signal propagation time from the experiment to the oscilloscope.

Good agreement between the analytical solution and the measurement, with deviations typically in the sub-percent range, is reached. Based on the time-of-flight measurements, the beam energy in the LEBT section can be monitored during full operation of the facility.

D. Wien ratio

A characteristic feature of the $E \times B$ setup is the necessity to match the magnetic and electric deflection forces. Therefore, the behavior of the chopper for different Wien ratios R_{Wien} of the electric to the magnetic field was investigated. The Wien ratio corresponds to the longitudinal velocity of the particles that can travel through the fields without transverse deflection.

For static fields in a hard-edge approximation, the Wien ratio is directly given by $R_{\mathrm{Wien}} = E_x \cdot B_y^{-1}$ [30]. For arbitrary field distributions and time-dependent electric fields, the Wien ratio has to be modified [3]:

$$R_{\mathrm{Wien}} = \frac{\int E_x dz \cdot f_{\mathrm{tof}}}{\int B_y dz}. \tag{6}$$

The time-of-flight factor f_{tof} has to be introduced in the equation because the finite flight time through the time-dependent electric field reduces the amplitude of the effective time-averaged electric field [3]. This correction is especially relevant for low-energy beams.

In practice, the Wien condition is determined by

$$R_{\mathrm{Wien}} = \frac{\int E_x dz \cdot f_{\mathrm{tof}}}{\int B_y dz} = \frac{\int E_{\mathrm{sim}} dz \cdot \frac{V_{\mathrm{meas}}}{V_{\mathrm{sim}}} \cdot f_{\mathrm{asym}} \cdot f_{\mathrm{tof}}}{\int B_{\mathrm{sim}} dz \cdot \frac{I_{\mathrm{meas}}}{I_{\mathrm{sim}}}}. \quad (7)$$

Here, the magnetic field B_{sim} is numerically computed for a coil current I_{sim} and is scaled with the measured dipole current I_{meas}. Then, the electric field E_{sim} is simulated for the given geometry using a static voltage V_{sim} and is scaled with the measured voltage pulse amplitude V_{meas}. The factor f_{asym} corrects a small measured asymmetry between the positive and the negative voltage pulse.

Figure 14 shows the measured charge that was transported in the pulse flat top $Q_{\mathrm{flattop}} = I_{\mathrm{BCT}}^{\mathrm{max}} \cdot t_{\mathrm{flattop}}$. It is plotted as a function of the Wien ratio R_{Wien}. For easier interpretation, the Wien ratio is normalized to the calculated velocity v_0 of the 14 keV helium ion beam.

In the experiment, the dipole current was kept constant while the voltage pulse amplitude V_{meas} was increased step by step. The amplitude $I_{\mathrm{BCT}}^{\mathrm{max}}$ and the flat-top length t_{flattop} of each beam pulse were measured.

The errors of the Wien ratio are calculated from the uncertainties of each factor in Eq. (7) while the error $\Delta Q_{\mathrm{flattop}}$ is dominated by the maximum time error of $\Delta t_{\mathrm{flattop}} = 10$ ns.

For high electric fields, the magnetic deflection is overcompensated and the beam is swept back and forth over the aperture, generating a double-peak pulse [3]. In these cases, the flat top and maximum current of the higher peak are evaluated.

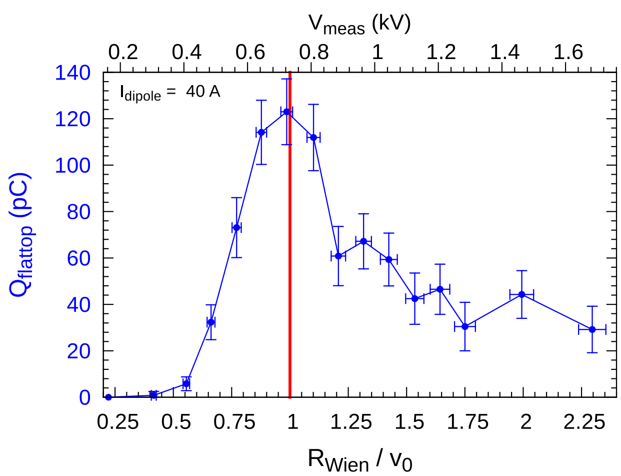

FIG. 14. Measured charge in the pulse flat top $Q_{\mathrm{flattop}} = I_{\mathrm{BCT}}^{\mathrm{max}} \cdot t_{\mathrm{flattop}}$ as a function of the Wien ratio R_{Wien}, which is normalized to the velocity v_0 of the 14 keV He^+ beam. The Wien ratio is varied by increasing the HV pulse amplitude V_{meas} while keeping the magnetic deflection field constant.

One can observe how the measured charge in the flat top Q_{flattop} reaches its maximum when the electric and magnetic deflection forces are accurately matched, i.e., close to the theoretically derived Wien condition $R_{\mathrm{Wien}}/v_0 = 1$.

VIII. CONCLUSION

The novel $E \times B$ chopper system for the low-energy line of the FRANZ facility was successfully designed, manufactured and installed. It was commissioned using a 14 keV He^+ beam. Repetition rates of 257 kHz and rise times of 120 ns were achieved.

The chopping concept is particularly suited for high-intensity applications where a high beam reliability is crucial. The $E \times B$ field configuration inverts and minimizes the duty cycle for the electric beam deflection, thus reducing the risk of voltage breakdowns. The concept combines the advantages of magnetic deflection, i.e., stable deflection without risks of voltage breakdown even at high beam intensities, and of electric deflection, i.e., operation with low power consumption even at high repetition rates. To ensure a high beam quality, the magnetic and electric deflection forces must be globally and locally matched. Therefore, magnetic shortening tubes were installed and the pole profile were shimmed in both the longitudinal and transverse plane.

For future high-current operations, a beam-separation system will securely dump the beam outside the beamline without high power deposition and uncontrolled production of secondary particles at the chopper aperture.

Since an $E \times B$ chopper acts as a pulsed velocity filter, certain molecular beam fractions or charge states can be separated from each other and the beam can be purified without using additional equipment in the beamline.

[1] S. Alzubaidi *et al.*, The Frankfurt neutron source FRANZ, Eur. Phys. J. Plus **131**, 124 (2016).

[2] C. Wiesner, L. P. Chau, M. Droba, N. Joshi, O. Meusel, I. Müller, and U. Ratzinger, Chopper for intense proton beams at repetition rates up to 250 kHz, in *Proceedings of the 23rd Particle Accelerator Conference, Vancouver, Canada, 2009* (IEEE, Piscataway, NJ, 2009), p. TU6PFP088.

[3] C. Wiesner, Dissertation, Johann Wolfgang Goethe-Universität Frankfurt am Main, 2014, http://publikationen.ub.uni-frankfurt.de/frontdoor/index/index/docId/36115.

[4] R. Reifarth, L. P. Chau, M. Heil, F. Käppeler, O. Meusel, R. Plag, U. Ratzinger, A. Schempp, and K. Volk, Opportunities for nuclear astrophysics at FRANZ, Pub. Astron. Soc. Aust. **26**, 255 (2009).

[5] M. Heilmann, C. Claessens, D. Mäder, O. Meusel, U. Ratzinger, A. Schempp, and M. Schwarz, A coupled RFQ-IH cavity for the neutron source FRANZ, in *Proceedings of*

the 4th International Particle Accelerator Conference, IPAC-2013, Shanghai, China, 2013 (JACoW, Shanghai, China, 2013), p. THPWO017.

[6] L. P. Chau, M. Droba, O. Meusel, D. Noll, U. Ratzinger, and C. Wiesner, Bunch compressor for intense proton beams, in *Proceedings of the 25th International Linear Accelerator Conference, LINAC-2010, Tsukuba, Japan* (KEK, Tsukuba, Japan, 2010), p. MOP100.

[7] W. Schweizer, U. Ratzinger, B. Klump, and K. Volk, A high intensity 200 mA proton source for the FRANZ-project (Frankfurt-Neutron-Source at the Stern-Gerlach-Center), Rev. Sci. Instrum. **85**, 02A743 (2014).

[8] J. Copley, Optimized design of the chopper disks and the neutron guide in a disk chopper neutron time-of-flight spectrometer, Nucl. Instrum. Methods Phys. Res., Sect. A **291**, 519 (1990).

[9] T. Unruh, J. Neuhaus, and W. Petry, The high-resolution time-of-flight spectrometer TOFTOF, Nucl. Instrum. Methods Phys. Res., Sect. A **580**, 1414 (2007).

[10] S. Itoh, K. Ueno, and T. Yokoo, Fermi chopper developed at KEK, Nucl. Instrum. Methods Phys. Res., Sect. A **661**, 58 (2012).

[11] J. Peters, J. Champion, G. Zsigmond, H. Bordallo, and F. Mezei, Using Fermi choppers to shape the neutron pulse, Nucl. Instrum. Methods Phys. Res., Sect. A **557**, 580 (2006).

[12] T. Adachi, T. Arai, K. W. Leo, K. Takayama, and A. Tokuchi, A solid-state Marx generator driven Einzel lens chopper, Rev. Sci. Instrum. **82**, 083305 (2011).

[13] J. Lackey, D. Bollinger, P. Karns, and C. Tan, A novel low energy fast chopper for H-injectors, Nucl. Instrum. Methods Phys. Res., Sect. A **701**, 194 (2013).

[14] Y. Mori, M. Muto, C. Ohmori, Y. Shirakabe, A. Takagi, and S. Yamaguchi, Test results of a fast beam chopper with MA cores, in *Proceedings of the 19th Particle Accelerator Conference, Chicago, IL, 2001* (IEEE, Piscataway, NJ, 2001), p. FPAH305.

[15] H. Liu, H. Ouyang, J. Peng, T. Huang, K. Gong, T. Xu, and S. Fu, Design and experiment results of the LEBT pre-chopper for CSNS, Nucl. Instrum. Methods Phys. Res., Sect. A **654**, 2 (2011).

[16] J. W. Staples, J. J. Ayers, D. W. Cheng, J. B. Greer, M. D. Hoff, and A. Ratti, The SNS four-phase LEBT chopper, in *Proceedings of the 18th Particle Accelerator Conference, New York, 1999* (IEEE, New York, 1999), p. WEA32.

[17] A. Shor, D. Berkovits, I. Fishman, A. Grin, B. Kaiser, and L. Weissman, Performance of beam chopper at SARAF via RF deflector before the RFQ, in *Proceedings of the 26th International Linear Accelerator Conference LINAC-2012, Tel-Aviv, Israel* (JACoW, Tel-Aviv, Israel, 2012), p. THPB094.

[18] L. Prost, R. Andrew, A. Chen, B. Hanna, V. Scarpine, A. Shemyakin, J. Steimel, and R. D'Arcy, Status of the PXIE low energy beam transport line, in *Proceedings of the 5th International Particle Accelerator Conference, IPAC-2014, Dresden, Germany* (JACoW, Dresden, Germany, 2014), p. MOPRI086.

[19] L. Neri, L. Celona, S. Gammino, D. Mascali, A. Caruso, A. Longhitano, L. Calabretta, B. Cheymol, and A. Ponton, The ESS low energy beam transport line design, in *Proceedings of the 26th International Linear Accelerator Conference LINAC-2012, Tel-Aviv, Israel* (JACoW, Tel-Aviv, Israel, 2012), p. THPB028.

[20] C. Wiesner, Diplomarbeit, Johann Wolfgang Goethe-Universität Frankfurt am Main, 2008.

[21] W. Posselt, U. Ratzinger, L. Rohrer, N. Gärtner, and E. Nolte, An 'emittance conserving' chopper for particle beams, Nucl. Instrum. Methods Phys. Res., Sect. A **236**, 37 (1985).

[22] P. Sigmund, Mechanisms and theory of physical sputtering by particle impact, Nucl. Instrum. Methods Phys. Res., Sect. B **27**, 1 (1987).

[23] P. B. Wilson, Frequency and pulse length scaling of RF breakdown in accelerator structures, in *Proceedings of the 19th Particle Accelerator Conference, Chicago, IL, 2001* (IEEE, Piscataway, NJ, 2001), p. ROAA012.

[24] M. Re, G. Cuttone, E. Zappal, and S. Passarello, Breakdown mechanisms in electrostatic deflector, in *Proceedings of the 16th International Conference on Cyclotrons and Their Applications* (AIP, Melville, NY, 2001), p. 151.

[25] J. Norem, A. Hassanein, Z. Insepov, and I. Konkashbaev, Breakdown in RF cavities, in *Proceedings of the 21st Particle Accelerator Conference, Knoxville, TN, 2005* (IEEE, Piscataway, NJ, 2005), p. TPPT025.

[26] A. Aleksandrov, C. Allen, S. Cousineau, V. Danilov, J. Galambos, D. Jeon, J. Holmes, T. Pelaia, M. Plum, A. Shishlo, M. Stockli, and Y. Zhang, Performance of the SNS front end and warm linac, in *Proceedings of the 11th European Particle Accelerator Conference, Genoa, 2008* (EPS-AG, Genoa, Italy, 2008), p. THPP073.

[27] U. Wienands, M. Sullivan, R. Akre, W. Cheng, W. Colocho, S. DeBarger, F.-J. Decker, S. Ecklund, A. Fisher, D. Kharakh, A. Krasnykh, and A. Novokhatski, High-current effects in the PEP-II storage rings, in *Proceedings of the 11th European Particle Accelerator Conference, Genoa, 2008* (EPS-AG, Genoa, Italy, 2008), p. WEPP041.

[28] Y. Kang, J. Wang, S. Milton, L. Teng, K. Thompson, J. Jones, D. Walters, and J. Jagger, Beam chopper for the low-energy undulator test line (LEUTL) in the APS, in *Proceedings of the Particle Accelerator Conference, Vancouver, BC, Canada, 1997* (IEEE, New York, 1997).

[29] C. Wiesner, L. P. Chau, H. Dinter, M. Droba, N. Joshi, O. Meusel, I. Müller, and U. Ratzinger, $E \times B$ chopper system for high intensity proton beams, in *Proceedings of the 25th International Linear Accelerator Conference, LINAC-2010, Tsukuba, Japan* (KEK, Tsukuba, Japan, 2010), p. THP071.

[30] W. Wien, Untersuchungen über die electrische Entladung in verdünnten Gasen, Ann. Phys. (Berlin) **301**, 440 (1898).

[31] C. Wiesner, L. P. Chau, H. Dinter, M. Droba, O. Meusel, I. Müller, D. Noll, and U. Ratzinger, Chopping high intensity proton beams using a pulsed Wien filter, in *Proceedings of the 3rd International Particle Accelerator Conference, New Orleans, LA, 2012* (IEEE, Piscataway, NJ, 2012), p. THPPP074.

[32] C. Wiesner, M. Droba, O. Meusel, D. Noll, O. Payir, U. Ratzinger, and P. Schneider, Chopping high-intensity ion beams at FRANZ, in *Proceedings of the 27th International*

Linear Accelerator Conference LINAC-2014, Geneva, Switzerland (JACoW, Geneva, Switzerland, 2014), p. WEIOB01.

[33] E. Gelfort, Das Separationsvermögen des Wien-Filters, Int. J. Mass Spectrom. Ion Phys. **14**, 349 (1974).

[34] R. L. Seliger, $E \times B$ mass-separator design, J. Appl. Phys. **43**, 2352 (1972).

[35] CST EM STUDIO, https://www.cst.com/Products/CSTEMS, rev. 2015-08-24.

[36] D. Noll, M. Droba, O. Meusel, U. Ratzinger, K. Schulte, and C. Wiesner, The particle-in-cell code bender and its application to non-relativistic beam transport, in *Proceedings of the 54th ICFA Advanced Beam Dynamics Workshop on High-Intensity, High Brightness and High Power Hadron Beams HB-2014, East-Lansing, MI, USA* (JACoW, East-Lansing, MI, USA, 2014), p. WEO4LR02.

[37] M. Reiser, *Theory and design of charged particle beams* (WILEY-VCH Verlag GmbH & Co. KGaA, Weinheim, 2004), Chap. 4.6.

[38] D. Noll, Dissertation, Johann Wolfgang Goethe-Universität Frankfurt am Main, 2016.

[39] C. A. Valerio-Lizarraga, I. Leon-Monzon, and R. Scrivens, Negative ion beam space charge compensation by residual gas, Phys. Rev. ST Accel. Beams **18**, 080101 (2015).

[40] A. BenIsmail, R. Duperrier, D. Uriot, and N. Pichoff, Space charge compensation studies of hydrogen ion beams in a drift section, Phys. Rev. ST Accel. Beams **10**, 070101 (2007).